Superconducting RFTES Detector at Milli-Kelvin Temperatures

Alexey V. Merenkov, Vladimir I. Chichkov, Andrey B. Ermakov, Alexey V. Ustinov, and Sergey V. Shitov

***Abstract*—We describe the first phase of experimental study of the superconducting bridge RFTES detector at temperatures 20–300 mK including the measurement of its thermal conductance, which fits the model of electron gas heating. We discuss the idea of the RFTES scheme, which is based on the probing of microwave loss near superconducting transition of the bridge. The heat applied to the bridge is generated by the probing signal at the frequency of the high-*Q* resonator. Since the real part is dominating in the nonlinear impedance of the bridge, the applied heat provides merely amplitude modulation of *Q* suggesting the suppression of phase jitter of the resonator. The bridge was made from a 50-nm-thick hafnium film ($T_C \approx 380$ mK) sized to 2.5 μm × 2.5 μm. The resonator and the rest of the circuit were made from 200-nm-thick film of niobium ($T_C \approx 9$ K) demonstrating the loaded *Q*-factor up to and above 10 000 at 1.5 GHz. A cryogenic semiconductor amplifier was used in the readout circuit. The thermal conductance was measured using the steady *Q* regime of the resonator and found to follow T^5 down to and below $G \approx 1\times10^{-13}$ W/K. The *NEP* below 10^{-18} W/$\sqrt{\text{Hz}}$ is estimated for the electron temperature of the bridge about 300 mK.**

***Index Terms*—Superconducting bolometer, transition edge sensor, high-Q resonator, superconducting film impedance.**

I. Introduction

NOWADAYS, astrophysics applications require imaging sensors containing more than 1000 pixels. To readout such arrays, the frequency domain multiplexing (FDM) is a good solution. It allows both to reduce complexity of construction of the detectors and to increase integration time for each pixel [1]. There are two types of advanced superconducting detectors: the microwave kinetic inductance detector (MKID) [2] and the transition edge sensor (TES) [3], [4]. The important benefit from an MKID array is simplicity of FDM using only one semiconductor RF amplifier. By contrast, TES bolometer can hardly be used without the delicate and costly SQUID amplifier, which band is limited to MHz frequencies. These facts do not favor a fully integrated readout circuit of a TES array. On the other hand, TES has the highest sensitivity among its class of detectors, so development of a TES array with integrated readout is of great practicable interest. Recently we have presented a niobium-based demonstrator of Radio-Frequency Transition Edge Sensor (RFTES) concept, suitable for imaging arrays, at temperatures 1.5−4.5 K with encouraging optical Noise Equivalent Power (*NEP*) down to $\sim 10^{-14}$ W/$\sqrt{\text{Hz}}$ that was measured with a blackbody radiation sources [5]–[7]. Here we present new evidence of good potential of the new approach at ultra-low temperatures along with more details for discussion started in [7].

Manuscript received February 18, 2018; revised March 19, 2018; accepted April 7, 2018. Date of publication April 17, 2018; date of current version May 8, 2018. This work was supported in part of theoretical and simulation study by the Ministry of Education and Science of the Russian Federation in the framework of Increase Competitiveness Program of the National University of Science and Technology MISiS, under Grant K2-2014-025; and in part by the Russian Science Foundation under Grant 17-19-01786 in part of fabrication samples and detailed experimental study. *(Corresponding author: Sergey V. Shitov.)*

A. V. Merenkov and V. I. Chichkov are with the National University of Science and Technology MISiS, Moscow 119049, Russia (e-mail: transcend_lexa@mail.ru; chichkov.vladimir@gmail.com).

A. B. Ermakov and S. V. Shitov are with the Institute of Radio Engineering and Electronics, Russian Academy of Sciences, Moscow 125009, Russia, and also with the National University of Science and Technology MISiS, Moscow 119049, Russia (e-mail: ermakov@hitech.cplire.ru; sergey3e@gmail.com).

A. V. Ustinov is with the Institute of Physics, Karlsruhe Institute of Technology, Karlsruhe D-76128, Germany, and also with the Russian Quantum Center, National University of Science and Technology MISiS, Moscow 119049, Russia (e-mail: ustinov@kit.edu).

Color versions of one or more of the figures in this paper are available online at http://ieeexplore.ieee.org.

Digital Object Identifier 10.1109/TASC.2018.2827981

II. Principle of TES Detector With RF Readout

A. Equivalent Scheme

To analyze the idea of the new microwave readout, the simplified schemes of TES and RFTES detectors are compared in Fig. 1(a) and (b), respectively. The resonant circuits play the role of an FDM-filter in both cases. The frequencies of scheme from Fig. 1(a) are limited to ∼1 MHz by the typical parameters: $R_{B1} \approx 1$ Ohm, $L_R \approx 10\,\mu$H and $C_R \approx 1$ nF [8]. The resulting *Q*-factor is relatively low, about 100, for the parameters above. It is much easier to achieve high-*Q* regime using scheme from Fig. 1(b): $Q \sim 10{,}000$ for $R_{B2} = 10$ Ohm, if $C_1/C_2 = 100$ and $C_1 + C_2 \approx C_R$. It is possible to demonstrate that the readout of RFTES detector can work, under certain conditions, the same way as one of a classical TES detector. The probing signal of RFTES is applied indirectly using the microwave transmission line. The line is weakly coupled via the common inductor L_C to a resonator, which is an open-ended quarter-wave coplanar waveguide (CPW) as shown in Fig. 1(c). The resonator plays the role of an impedance transformer. It converts the 50 Ohm of the microwave probing source/LNA to a shunt resistance in parallel to the bridge, $R_{SH} << R_{B1}$, exactly as it is required for a classical TES. It is important to note here that the bridge performs roles of both the absorber and the thermometer. We assume that the probing signal is principally invasive. It pre-heats the bolometer's "absorbing body" from the bath temperature $T_{\text{bath}} < T_c$ towards the best temperature range of its "thermometer". A THz signal from the antenna is slightly changing

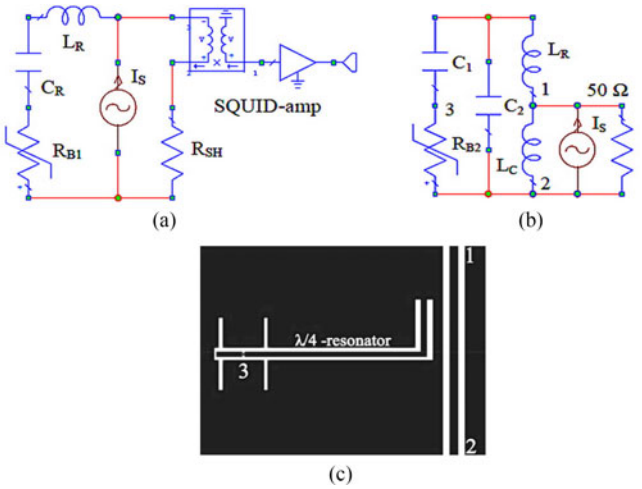

Fig. 1. Principle of an RFTES detector: (a) typical FDM scheme of a classical TES detector with low-frequency SQUID amplifier; (b) scheme of RFTES detector probed with a 50-Ω source at ports 1 and 2 of a throughtput line; the resonator is loaded with absorber R_{B2} at port 3; (c) simplified layout of RFTES chip with double-slot THz antenna integrated with the resonator; ports 1, 2 and 3 are in accordance with (b).

the temperature of the bridge. The impedance of the detector grows and changes the *Q*-factor of the microwave resonator that is measured as variation of S_{21}.

B. Microwave Impedance

The impedance control and readout are the key issues for the new device. There are at least three theories describing impedance of a superconductor at microwave frequencies: the Gorter-Kazimir two-fluid model [9], the Mattis-Bardeen theory [10] and the Abrikosov-Gor'kov-Khalatnikov theory [11]. They predict two important effects at growing frequency f_0: 1) the impedance temperature response is degrading meaning lower *dZ(T, f)/dT*; and 2) the active impedance is present at temperatures well below T_C. We established a criterion for the upper frequency limit, f_0. Since an experimental low-frequency curve *R(T)* is never as sharp as the theoretical one, there must be a frequency, f_0, at which the theoretical $dZ(T, f_0)/dT$ is comparable to experimental *dR/dT*. For the frequencies above f_0, reduction of *dZ(T, f)/dT* is unavoidable, and the bolometer's efficiency can decrease, demanding for an ultra-low-noise RF amplifier. To estimate the effect, we use the Mattis-Bardeen theory at Pippard's limit. The hafnium was chosen as the material for the micro-bridge due to $T_C \approx 0{,}38$ K. The normalized active impedance *R(T, ω)* was calculated using the following equations from [10]:

$$\frac{R}{R_N} = \frac{\sigma_1 \cdot \sigma_N}{\sigma_1^2 + \sigma_2^2} \tag{1}$$

$$\frac{\sigma_1}{\sigma_N} = \frac{2}{\hbar\omega}\int_{\Delta(T)}^{\infty}(f(u) - f(u+\hbar\omega))g(u)du + \frac{1}{\hbar\omega}\int_{\Delta(T)-\hbar\omega}^{-\Delta(T)}(1-2f(u+\hbar\omega))g(u)du \tag{2}$$

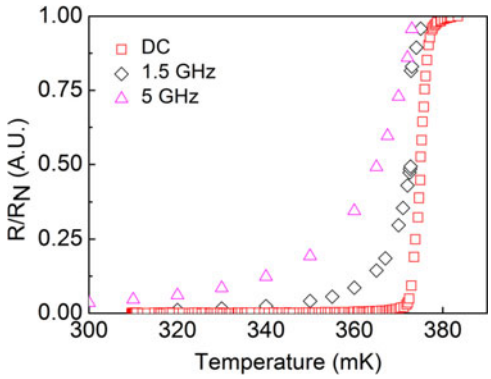

Fig. 2. Calculated real part of impedance of hafnium for a few frequencies in comparison to experimentally measured *R(T)* (boxes): 1.5 GHz (diamonds), 5 GHz (triangles).

$$\frac{\sigma_2}{\sigma_N} = \frac{1}{\hbar\omega}\int_{\Delta(T)-\hbar\omega,-\Delta(T)}^{\Delta(T)} \times \frac{(1-2f(u+\hbar\omega))(u^2+\Delta(T)^2+\hbar\omega u)du}{\sqrt{\Delta(T)^2-u^2}\cdot\sqrt{((u+\hbar\omega)^2-\Delta(T)^2)}} \tag{3}$$

Here $f(u)$ is the Fermi-Dirac function and *g(u)* substitutes for

$$g(u) = \frac{u^2+\Delta(T)^2+\hbar\omega u}{\sqrt{u^2-\Delta(T)^2}\cdot\sqrt{(u+\hbar\omega)^2-\Delta(T)^2}} \tag{4}$$

The second term of (2) does not appear unless the photon energy is relatively large, $\hbar\omega > 2\Delta(T)$. For the large photon energy the lower limit of the integral in (3) is $-\Delta(T)$ instead of $\Delta(T) - \hbar\omega$. The temperature dependence of energy gap is solved from the following equation [12]:

$$\frac{1}{N(0)\cdot V} = \int_0^{\hbar\omega_D}\frac{th\left(\frac{\sqrt{\xi^2+\Delta(T)^2}}{2k_BT}\right)}{\sqrt{\xi^2+\Delta(T)^2}} \tag{5}$$

here *N(0)* is the density of Bloch states of one spin per unit energy at the Fermi surface, ξ is Bloch energy, ω_D is Debye frequency. The calculated impedance is compared with the experimentally measured *R(T)* as presented in Fig. 2. The frequency of 1.5 GHz is chosen as the design parameter for the experimental study described below.

III. Experimental Details

A. Layout, Fabrication, and Experimental Setup

We designed two layouts and fabricated three types of chips tuned to the same frequency (1.5 GHz). Two chips have no sensing bridge, and they are used as a reference. One of the reference chips included a λ/4 resonator made of homogenous CPW as shown in Fig. 3(a). Another reference chip presents the full-structured detector with the double-slot antenna as shown in Fig. 3(b) except the bridge, which is a Nb dummy. The resonators and the remaining parts of the circuits are made from a 100-nm niobium film ($T_C \approx 9$ K). The third chip contains the

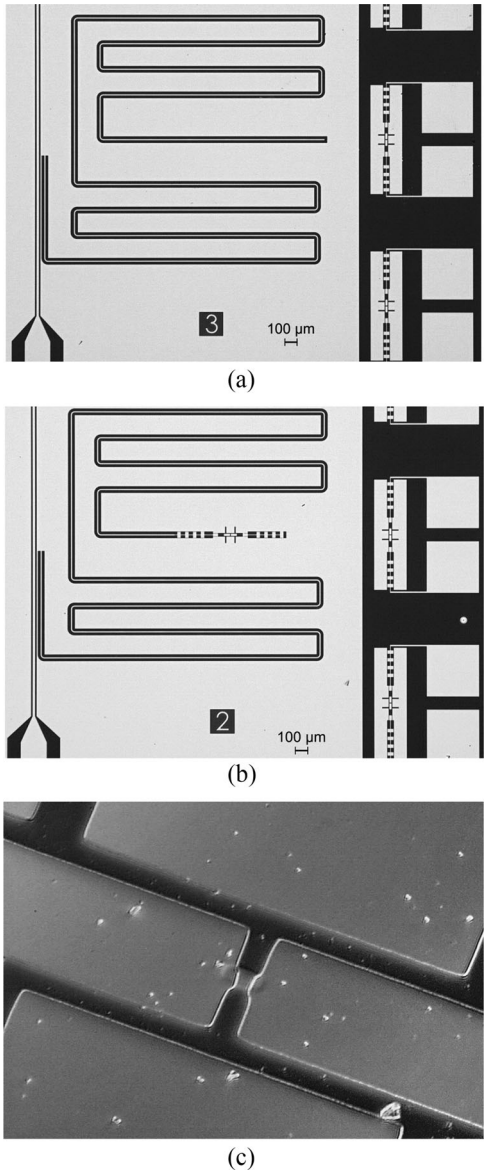

Fig. 3. Photo of experimental layouts designed for 1.5 GHz: (a) folded reference resonator without inhomogeneity; (b) full-structutred sample with dummy bridge made from Nb; (c) hafnium bridge (2.5 μm $\times$ 2.5 μm) embedded into structure (b).

bridge made from 50-nm thick hafnium film that is shown in Fig. 3(c).

The chips are fabricated using the mask-free laser lithographer Heidelberg μPG 501. The niobium (99.99%) and hafnium (99.99%) targets are sputtered onto a 500-μm silicon substrate using the DC-magnetron at the following conditions: the base pressure was (8–9)$\cdot 10^{-8}$ mbar, the operating pressure of Ar-gas was $5\cdot 10^{-3}$ mbar. The sputtering rate was 22 nm/min for Nb and 28 nm/min for Hf. All patterns were formed using standard lift-off process.

We use 4-K close-cycle cryostat to study the reference chips and the 20-mK dilution fridge for the sample with the hafnium bridge. The S_{21} parameter of the path inside the cryostat was measured at different probing powers. The low-temperature path inside both cryostats was approximately the same. The series

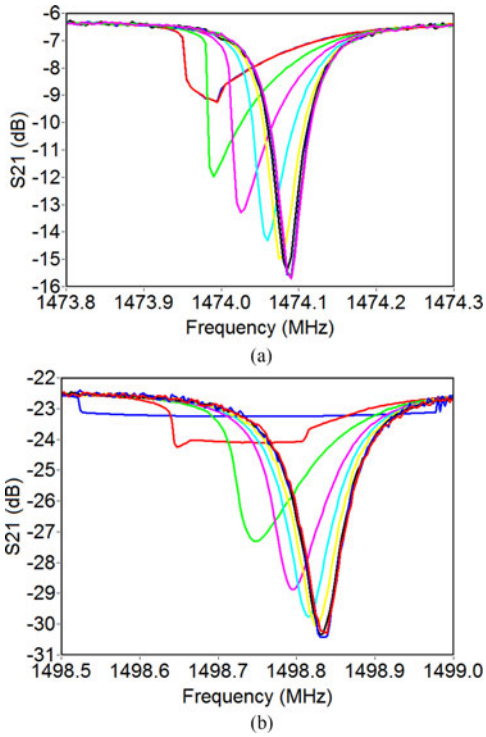

Fig. 4. Experimental data on transmission of reference chips at probing powers $-80\ldots+3$ dBm; curve families are qualitative: (a) S_{21} for chip from Fig. 3(a); and (b) S_{21} for chip from Fig. 3(b). Nonlinear effects at incident powers >-30 dBm (referred to the chip) are signatures of growing kinetic inductance of superconducting resonators. Note that different attenuators were used for the above data.

chain included: 1) coaxial attenuator (up to 40 dB) at the temperature of the chip; 2) the chip bonded with ports 1 and 2 to the intermediate PCB; and 3) a chain of two RF-isolated cryogenic semiconductor amplifiers installed at a more powerful 4-K stage of the cryostat (gain up to 40 dB at 1.5 GHz). Fig. 4 demonstrates that reference chips of different design show resonance dip near the nominal frequency of 1.5 GHz tolerating for less than 2%. At this point we may state adequate accuracy of our EM-design.

B. Experimental Results and Discussion

The third chip with sensing bridge shown in Fig. 3(c) was tested within temperature range 20–300 mK. Assuming that the hafnium bridge is in superconducting state, at 50 mK, we fitted parameters of the lumped circuit from Fig. 1(b) to S_{21}-data measured at "nearly zero" incident power that was about -120 dBm. The extracted *linear* parameters of the circuit are: $L_R = 3.4$ nH; $L_C = 0.035$ nH; $C_1 = 0.092$ pF; $C_2 = 3.31$ pF.

To estimate the bolometric sensitivity, *NEP*, the rate of heat escape from the electron subsystem can be described in terms of thermal conductance, G. For a steady electron temperature T_{e0} the equation for the heat balance can be written as

$$P_1 - P_2 = (T_{e0} - T_1)\cdot G_s - (T_{e0} - T_2)\cdot G_s \qquad (6)$$

where T_1 and T_2 are a pair of different bath temperatures, P_1 and P_2 are corresponding powers, and G_s characterizes the static thermal conductance. One may assume that the steady

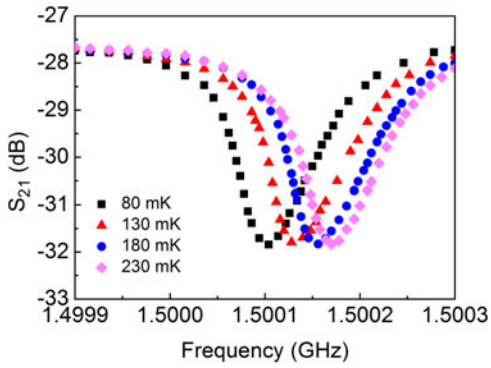

Fig. 5. Experimental data on microwave heating of hafnium bridge: the regime of steady loss (constant dip ΔS_{21} in coefficient of transmission S_{21}) at different temperatures and microwave powers listed in Table I. Note that frequency shift is not detector response. It corresponds to different bath temperatures, and the anomalous direction of the frequency shift is not understood yet.

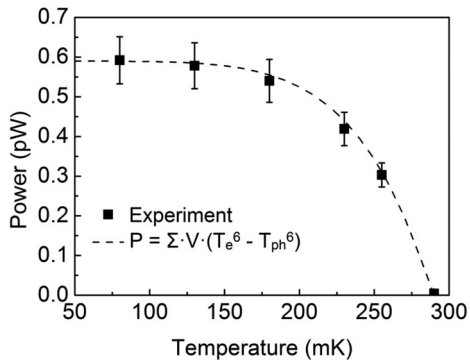

Fig. 6. Best fit of (7) (dashed curve) to experimental data from Fig. 5 (bar points) at different temperatures (also listed in Table I).

TABLE I
THERMAL CONDUCTANCE, G, AND SENSITIVITY, *NEP*

Data Set # →	1	2	3	4	St. dev.
T_i (mK)	80	130	180	230	5
P_i (pW)	0.592	0.578	0.54	0.419	0.04
ΔS_{21} (dB)	-4.43	-4.37	-4.415	-4.42	0.023
G_s (pW/K)	2.828	3.649	5.01	7.316	-
NEP_s (aW/√Hz)	3.686	4.187	4.906	5.928	-
G_d (pW/K)	0.02	0.226	1.148	3.91	-
NEP_d (aW/√Hz)	0.309	1.04	2.348	4.334	-

T_{e0} means steady loss (resistance) of the bridge and also steady Q-factor. In other words, the same temperature of electron system means constant dip of transmission coefficient, S_{21}. In our experiment we achieved such steady condition for a number of temperatures as shown in Fig. 5.

It is worth to note here that the exact value of T_{e0} is not needed in (6), but it *must* be steady. We have estimated T_{e0} experimentally at "nearly zero" incident power as 280 . . . 300 mK. In spite this method is straightforward, the (6) can be inaccurate if G_s is temperature sensitive or the temperature points are far apart. A more accurate estimate of G can be done using above steady-state measurements along with relation between the electron-phonon exchange power and corresponding temperatures. According to number of previous publications, for example [13], [14], thermal conductance for hafnium films can

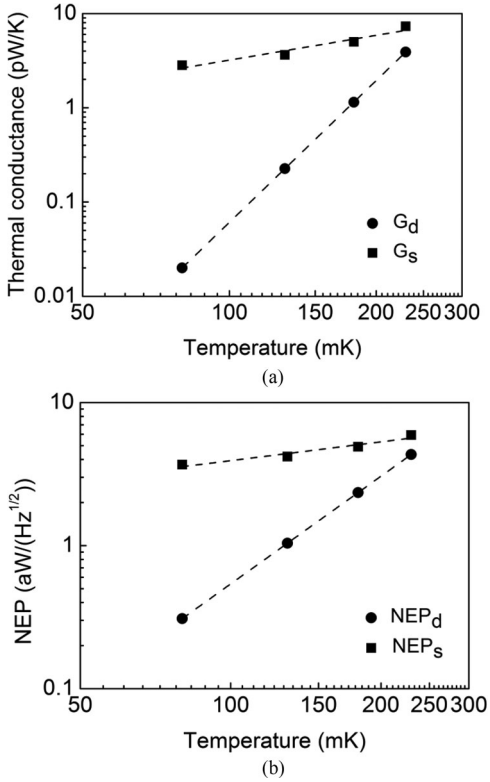

Fig. 7. Evaluation of experimental data. (a) Thermal conductance of the hafnium bridge based on data from Fig. 5: G_s calculated from (6) as a static difference and G_d calculated from (8) as a differential. (b) *NEP* calculated for a resistive bolometer at temperature $T_{e0} = 295$ mK using (9) with either G_d or G_s.

be approximated as

$$P_{e-ph} = \Sigma \cdot V \cdot (T_e^n - T_{ph}^n) \tag{7}$$

We have used fitting of (7) to our experimental data aiming for the material parameter Σ. The best fit is shown in Fig. 6 for $n = 6$ and $\Sigma = (13.5 \pm 2) \times 10^8$ W/(m^{3}K^6). This value for Σ is about twice larger than 5.5×10^8 W/(m^{3}K^6) evaluated using data from reference [14] that can be explained by additional (uncalibrated) loss in the RF cables. Since the fit errors are about to overlap, it is possible to conclude on a very reasonable agreement with the data from [14]. The value $T_{e0} = 283 \pm 5$ mK is also found via the fit being in a good agreement with the abovementioned experimental "zero-power" data. We assume that Kapitsa resistance is negligible, so phonon temperature equals bath temperature ($T_{ph} \approx T_{\rm bath}$).

Since the fitting coefficients are available, the accurate value of thermal conductance can be calculated via differential of (7)

$$G_d(T_{ph}) = 6 \cdot \Sigma \cdot V \cdot T_{ph}^5 \tag{8}$$

The G_d and G_s are essentially different as listed in Table I. Over-estimating value of thermal conductance while using G_s, one under-estimates *NEP* benefiting from no need for any knowledge on parameters of the bridge material. The potential sensitivity of the bolometric device can be calculated using the classical formula for a purely resistive bolometer

$$NEP_i = \sqrt{4k_B G_i {T_{e0}}^2} \tag{9}$$

and presented in Fig. 7(b) and Table I for both $G_i = G_s$ and $G_i = G_d$. The estimated *NEP* data are quite encouraging, since the atto-Watt-range sensitivity can be expected at temperatures about 300 mK.

IV. Conclusion

We used the Mattis-Bardeen theory and estimated the feasibility limit for the probing frequency of RFTES based on *hafnium* micro-bridge as 1-2 GHz. We experimentally verified accuracy of our EM-design methods with reference niobium resonators ($Q \approx 10^4$) and demonstrated smooth response of Q-factor using a *hafnium* bridge at 1.5 GHz. These microwave measurements allowed us to find thermal conductivity of the bridge, G, using the novel method of steady microwave loss. The experimental data support the electron gas model for $G \sim T^5$ being in a good agreement with existent data. The model of purely thermal noise yields *NEP* below 10^{-18} W/$\sqrt{\text{Hz}}$ that is promising for the future FDM arrays made of RFTES detectors. To confirm these data, a test of optical sensitivity is planned as the next phase of the study.

References

[1] T. M. Lantinga *et al.*, "Frequency domain multiplexing for large scale bolometer arrays," *Proc. SPIE*, vol. 4855, pp. 172–181, 2003.

[2] P. K. Day, H. G. LeDuc, B. A. Mazin, A. Vayonakis, and J. Zmuidzinas, "A broadband superconducting detector suitable for use in large arrays," *Nature*, vol. 425, pp. 817–821, 2003.

[3] K. D. Irwin and G. C. Hilton, "Transition-edge sensors," *Topics Appl. Phys.*, vol. 99, pp. 63–149, 2005.

[4] W. Holland, "SCUBA-2: A 10,000-pixel submillimeter camera for the James Clerk Maxwell Telescope," *Proc. SPIE*, vol. 6275, 2006, Art. no. 62751E.

[5] S. V. Shitov *et al.*, "Wide-range bolometer with RF readout TES," *IEEE Trans. Appl. Supercond.*, vol. 25, no. 3, Jun. 2015, Art. no. 2101704.

[6] S. V. Shitov *et al.*, "Progress in development of the superconducting bolometer with microwave bias and readout," *IEEE Trans. Appl. Supercond.*, vol. 27, no. 4, Jun. 2017, Art. no. 2100805, doi: 10.1109/TASC.2017.2655507.

[7] A. A. Kuzmin *et al.*, "Development of TES bolometers with high-frequency readout circuit," *IEEE Trans. THz Sci. Technol.*, vol. 3, no. 1, pp. 25–31, Jan. 2013.

[8] K. D. Irwin, "Shannon limits for low temperature detector readout," *AIP Conf. Proc.*, vol. 1185, 2009, Art. no. 229.

[9] C. J. Gorter and H. B. G. Casimir, "Thermodynamics of the superconducting state," *Z. Phys.*, vol. 15, pp. 539–542, 1934.

[10] D. C. Mattis and J. Bardeen, "Theory of the anomalous skin effect in normal and superconducting metals," *Phys. Rev.*, vol. 111, pp. 412–417, 1958.

[11] A. A. Abrikosov, L. P. Gor'kov, and I. M. Khalatnikov, "Analysis of experimental data relating to the surface impedance of superconductor," *Sov. Phys.–JETP*, vol. 37, no. 10, pp. 132–134, 1960.

[12] J. Bardeen, L. N. Cooper, and J. R. Schrieffer, "Theory of superconductivity," *Phys. Rev.*, vol. 108, no. 5, pp. 1175–1204, 1957.

[13] F. C. Wellstood, C. Urbina, and J. Clarke, "Hot-electron effects in metals," *Phys. Rev. B*, vol. 49, pp. 5942–5955, 1994.

[14] M. E. Gershenson, D. Gong, and T. Sato, "Millisecond electron-phonon relaxation in ultrathin disordered metal films at millikelvin temperatures," *Appl. Phys. Lett.*, vol. 79, 2001, Art. no. 2049.